IEEE Control Systems Letters paper presented at
2023 American Control Conference (ACC)
San Diego, CA, USA. May 31 - June 2, 2023

A Two-Layer Human-in-the-Loop Optimization Framework for Customizing Lower-Limb Exoskeleton Assistance

Siqi Zheng, Student Member, *IEEE* and Ge Lv*, Member, *IEEE*

***Abstract*— Task-invariant control paradigms can enable lower-limb exoskeletons to provide assistance for their users across various locomotor tasks without prescribing to specific joint kinematics. As an energetic control method, energy shaping can alter a human's body energetics in the closed-loop to provide gait benefits. To obtain the energy shaping law for underactuated systems, a set of nonlinear partial differential equations, called the matching condition, needs to be solved to determine the achievable closed-loop dynamics. However, solving matching conditions for high-dimensional nonlinear systems is generally difficult. In addition, how to define parameters for the closed-loop dynamics that render the optimal exoskeleton assistance remains unclear. In this paper, we proposed a two-layer, human-in-the-loop optimization framework for lower-limb exoskeletons to customize their assistance to human users. The inner-layer optimization finds solutions to the matching condition, meanwhile following the energy trajectories of a virtual reference model defined based on the self-selected gaits of humans and a scaled version of their anatomical parameters. The outer-layer incorporates human-in-the-loop Bayesian Optimization to update reference energy's parameters for reducing metabolic costs. Simulation results on two biped models demonstrate that the proposed framework can solve matching conditions numerically at the selected timestamps and the associated energy shaping strategies can reduce human metabolic cost. Moreover, exoskeletons torques calculated using an able-bodied subject's kinematic data well match human biological torques.**

I. INTRODUCTION

Lower-limb exoskeleton's control paradigms can be divided into two broad categories, i.e., enhancing physical abilities for able-bodied subjects and assisting individual with disabilities [1]. Most exoskeleton control methods for movement assistance and rehabilitation are designed for tasks to be carried out in a specific environment based on a particular task [2]. These task-specific control approaches are designed to follow certain trajectories that cannot be easily changed across subjects and locomotor tasks. Once the locomotor task changes, the exoskeleton needs to identify this change via pattern recognition systems and selects the corresponding new trajectory. This makes task-specific control algorithms more effective in gait rehabilitation that requires repetitive movements [3]. Different from gait rehabilitation, exoskeletons designed for assisting volitional human motion should be able to accommodate different daily activities [4], which cannot be captured by the current control paradigms.

Trajectory-free, task-invariant paradigms could provide more flexibility to allow volitional human motion and possibly eliminate the need to switch between multiple trajectories [1]. As one example, human muscle activation can be measured via Electromyography (EMG) sensors and used as feedback signals for exoskeleton control design to assist human locomotion [5], [6]. However, performance of EMG sensors is suspectable to measurement noises, placement of electrodes, and sweating [7]. Although there exist other control paradigms that are trajectory-free, they are specifically designed for dedicated tasks such as sit-to-stand [8] and stair ascent [9]. Energy shaping and passivity-based control paradigms [10], [11] can enable exoskeletons to provide task-invariant assistance by reducing the user's perceived body weight without knowledge from reference kinematic trajectories, therefore have the potential to provide consistent assistance across different daily activities.

While prior research on energy shaping has demonstrated beneficial results, two problems remain unsolved. The first one is the difficulty in solving matching conditions for high-dimensional systems with varying degrees of underactuation. To obtain an energy shaping control law for underactuated systems, the matching condition, which is a set of nonlinear partial differential equations (PDEs), needs to be solved to determine achievable closed-loop dynamics. To tackle this problem, previous studies [12], [13] managed to simplify nonlinear PDEs into quadratic or linear PDEs. However, these approaches either rely on assumptions that the shape variables being cyclic in the mass matrix [13] or mechanical energy is only dependent on actuated coordinates [12]. The associated theorems have only been applied to simple systems such as an inverted pendulum on a cart [14] and the beam-ball system [15]. These simplification methods cannot be applied to complex human-exoskeleton dynamics, which often include multiple degrees of freedom (DoFs) and the associated mass matrix is dependent on shape variables in general. While Lv et al. proposed the equivalent constrained dynamics in [16] to simplify the satisfaction of matching condition, the obtained solutions only form a subset of the entire solution set.

The second problem appears to be the choices of closed-loop dynamics that can lead to beneficial gait effects. Human-in-the-loop (HIL) optimization [17]–[20] has been applied to customize parameters for exoskeleton assistance to reduce metabolic costs. By measuring human respiratory data in real-time, algorithms such as Covariance Matrix Adaptation Evolution Strategy [19] and Bayesian Optimization (BO)

"*" indicates corresponding author

This work was supported by the South Carolina Translational Research Improving Musculoskeletal Health Faculty Development Award.

G. Lv is with the Departments of Mechanical Engineering and Bioengineering, S. Zheng is with the Department of Automotive Engineering. Clemson University, Clemson, SC 29634. Contact: {szheng2, glv}@clemson.edu

Authorized licensed use limited to: CLEMSON UNIVERSITY. Downloaded on February 19,2024 at 20:01:40 UTC from IEEE Xplore. Restrictions apply.

[18] were applied to customize parameters of human joint torque profiles for minimizing metabolic costs during walking. Similarly, Gordon et al. leveraged musculoskeletal modeling techniques to evaluate simulated metabolic cost metrics online so that the convergence speed of HIL optimization can be greatly increased [20]. Reinforcement Learning has also been applied to update an impedance controller's parameters for tracking desired knee trajectories [17] or customize control parameters of assistive torque profiles [21]. However, most of these methods aim to optimize the parameterized assistance torque for a specific activity. It is unclear if these proposed methods can be translated into other locomotor tasks and receive the same outcome through customizing the same parameters of a given torque profile. A paradigm shift from task-specific, trajectory-based customization to task-invariant, trajectory-free customization is needed for lower-limb exoskeletons to assist volitional human motion.

To address these two issues, we proposed a two-layer HIL optimization framework that can numerically solve the matching condition at selected points along a human-selected trajectory and customize closed-loop human energetics to generate optimal exoskeleton assistance. In the inner layer, we find solutions to the matching conditions at selected timestamps and track a reference energy. This reference energy is defined based on a reference model, whose states are defined based on a human user's self-selected gaits and its inertial parameters are scaled versions of real human anatomical parameters. Between two adjacent timestamps, we used a Gaussian process regression (GPR) model to interpolate the solutions to the matching condition and calculate the corresponding torques. The outer layer optimizes the parameters of the reference energy to minimize the metabolic costs of human walking through BO. The rest of the paper is organized as follows: Sec. II introduces the biped's dynamics and reviews energy shaping control. Sec. III puts forward the two-layer optimization framework. Sec. IV demonstrates the simulation results on two biped models and simulated exoskeleton torques based on an able-bodied subject's kinematic data. Finally, we draw conclusions and discuss future research directions in Sec. V.

II. Dynamics and Energy Shaping Review

A. Biped Dynamics

A human wearing an exoskeleton is modeled as a kinematic chain from the stance leg to the swing leg with respect to an inertial reference frame (IRF) [16]. We added a torso to the biped due to its positive effect on maintaining human walking stability [22]. The equation of motion (EoM) of an n-DoF biped can be expressed as

$$M\ddot{q} + C\dot{q} + N + A^T\lambda = \tau, \tag{1}$$

where $q \in \mathbb{Q}$ is the generalized coordinates vector with $\mathbb{Q}$ being the configuration space, $\dot{q}$ and $\ddot{q}$ are the corresponding angular velocity and acceleration vectors, $M \in \mathbb{R}^{n\times n}$ is the inertia matrix, $C \in \mathbb{R}^{n\times n}$ is the Coriolis/centrifugal matrix, and $N \in \mathbb{R}^n$ is the gravitational forces vector. The input torque $\tau = \tau_{\text{hum}} + \tau_{\text{exo}}$ consists of the human input $\tau_{\text{hum}} = Hv$ and the exoskeleton input $\tau_{\text{exo}} = Bu$, where $B = [0_{m\times(n-m)}, I_{m\times m}]^T \in \mathbb{R}^{n\times m}$ and $H = [0_{p\times(n-p)}, I_{p\times p}]^T \in \mathbb{R}^{n\times p}$ are matrices that map the exoskeleton actuator torque $u \in \mathbb{R}^m$ and the human joint torque $v \in \mathbb{R}^p$ into the overall dynamics. The term $A \in \mathbb{R}^{c\times n}$ is the constraint matrix defined by taking the gradient of c holonomic contact constraints and λ is the associated Lagrange multiplier [23]. During human walking, holonomic contact constraints vary in different gait phases that result in different A and λ. In [16], Lv et al. introduced equivalent constrained dynamics by plugging the expression of $A^T\lambda$ into (1) to generate a unified biped model across gait phases. The equivalent constrained dynamics can be expressed as

$$M_\lambda\ddot{q} + C_\lambda\dot{q} + N_\lambda = B_\lambda u + H_\lambda v, \tag{2}$$

where detailed definitions for all the dynamic terms can be found in [16].

B. Energy Shaping Control

Assuming an energy shaping control law exists (i.e., the matching condition is satisfied), it can shape the original dynamics (1) into the desired form

$$\tilde{M}\ddot{q} + \tilde{C}\dot{q} + \tilde{N} + A^T\tilde{\lambda} = \tilde{H}v, \tag{3}$$

where $\tilde{M}$, $\tilde{C}$, $\tilde{N}$, $\tilde{\lambda}$, and $\tilde{H}$ are dynamic terms in the closed-loop. Prior studies [16] show that compensating for human's inertial parameters is beneficial in assisting human gaits. In this paper, we define the terms $\tilde{M}$, $\tilde{C}$ and $\tilde{N}$ by scaling the inertial parameters of the human and exoskeleton as $\tilde{m}_i = k_i \cdot m_i$, $\tilde{I}_i = k_i \cdot I_i$, $k_i > 0$, where (m_i, I_i) are the inertial parameters of link i in the original dynamics (1). Note that we are not confining k_i to be a constant, but rather a function of the system's states over time.

Given (2), the desired equivalent constrained dynamics in the closed loop can be expressed as

$$\tilde{M}_\lambda\ddot{q} + \tilde{C}_\lambda\dot{q} + \tilde{N}_\lambda = \tilde{H}_\lambda v, \tag{4}$$

where $\tilde{M}_\lambda$, $\tilde{C}_\lambda$, $\tilde{N}_\lambda$ and $\tilde{H}_\lambda$ are defined similarly to the terms in (2) but with scaled inertial parameters. We showed in our prior research [23] that the closed-loop dynamics (4) and (3) are equivalent, i.e., shaping (1) into (3) is equivalent to shaping (2) into (4).

When a system is underactuated, the matching condition needs to be satisfied to determine achievable closed-loop dynamics with limited actuators [12]. Based on the equivalent constrained dynamics (2) and its desired form (4), the matching condition can be expressed as [16]

$$\begin{aligned} B_\lambda^\perp[M_\lambda\tilde{M}_\lambda^{-1}(\tilde{H}_\lambda v - \tilde{C}_\lambda\dot{q} - \tilde{N}_\lambda) \\ + C_\lambda\dot{q} + N_\lambda - H_\lambda v] = 0, \end{aligned} \tag{5}$$

where $B_\lambda^\perp \in \mathbb{R}^{(n-m)\times n}$ is the full-rank left annihilator of B_λ, i.e., $B_\lambda^\perp B_\lambda = 0$ and $\text{rank}(B_\lambda^\perp) = (n-m)$ [12]. Once the matching condition (5) is satisfied, the control law that shapes (2) into (4) can be expressed as

$$\begin{aligned} u = (B_\lambda^T B_\lambda)^{-1} B_\lambda^T [C_\lambda\dot{q} + N_\lambda - H_\lambda v \\ - M_\lambda\tilde{M}_\lambda^{-1}(\tilde{C}_\lambda\dot{q} + \tilde{N}_\lambda - \tilde{H}_\lambda v)]. \end{aligned} \tag{6}$$

Authorized licensed use limited to: CLEMSON UNIVERSITY. Downloaded on February 19,2024 at 20:01:40 UTC from IEEE Xplore. Restrictions apply.

III. Optimization framework formulation

This section introduces a two-layer optimization framework that incorporates HIL optimization for customizing energy shaping strategies, where the overall structure is shown in Fig. 1. When a dynamic system has multiple DoFs, solving matching condition (5) in real-time is a great challenge. Instead of obtaining its closed-form solutions, we try to solve the matching condition at selected timestamps t_j numerically. At a given state q, matrices M_λ, C_λ and N_λ are constants, and the closed-loop terms $\tilde{M}_\lambda$, $\tilde{C}_\lambda$ and $\tilde{N}_\lambda$ are matrices of $\tilde{m}_i$ and $\tilde{I}_i$. In other words, the matching condition (5) becomes a linear matrix equation at selected states, which is easier to solve compared to PDEs. The overall framework consists of two layers: an inner layer that aims to find solutions to the matching condition at selected timestamps meanwhile tracking the reference energy from a virtual reference model, and an outer layer that customizes the parameters of the reference energy to minimize energy expenditure.

A. Virtual Reference Model

To construct this framework, we will first need to define the virtual reference model. The reference model has the same configuration vector as (1), i.e.,

$$M_{\text{ref}}\ddot{q} + C_{\text{ref}}\dot{q} + N_{\text{ref}} + A^T\lambda_{\text{ref}} = \tau_{\text{hum}}, \tag{7}$$

where M_{ref}, C_{ref}, and N_{ref} are defined similarly to the terms in (1) but with a scaled version of human inertial parameters:

$$m_i^{\text{ref}} = \alpha_i \cdot m_i,\ I_i^{\text{ref}} = \alpha_i \cdot I_i. \tag{8}$$

Parameters m_i, I_i, and α_i are the mass, inertia, and reference model parameter of the i-th human link, respectively. We will specify the choices of α_i for different biped models in Sec. IV. Note that q and $\dot{q}$ in (7) are identical to the ones in (2), i.e., both are from an individual's self-selected gaits. Faraji et al. showed that changing mass of different body segments has different effects on human metabolic cost [24]. We therefore chose to define inertial terms in (7) with scaled inertial parameters, hoping the energy shaping law will enable exoskeletons to shape human body energetics for mimicking the behaviors of reference model (7).

B. Inner Layer Optimization

The inner layer tries to find k_i to satisfy the matching conditions (5) and track the reference model's energy at selected timestamp t_j. The closed-loop inertial parameters $\tilde{m}_i$ and $\tilde{I}_i$ of (4) are defined as

$$\tilde{m}_i = k_i(q(t_j), \dot{q}(t_j)) \cdot m_i,\ \tilde{I}_i = k_i(q(t_j), \dot{q}(t_j)) \cdot I_i, \tag{9}$$

where $k_i \geq 0$ is a function of the state $(q(t_j), \dot{q}(t_j))$. At selected timestamp t_j, the inner layer optimization is formulated as

$$\begin{aligned} \min_{k_i \in [K_{\min},\ K_{\max}]} \quad & f_{\text{inner}} = (E_{\text{ref}} - E_{\text{closed}})^2, \\ \text{s.t.} \quad & B_\lambda^\perp[C_\lambda\dot{q} + N_\lambda - M_\lambda\tilde{M}_{\lambda k_i}^{-1}(\tilde{C}_{\lambda k_i}\dot{q} + \tilde{N}_{\lambda k_i})] = 0, \\ & B^\perp(H_\lambda - M_\lambda\tilde{M}_{\lambda k_i}^{-1}\tilde{H}_{\lambda k_i})v = 0, \\ & |\tau_{\text{exo}}| < \text{sat}, \end{aligned}$$

where $\tilde{M}_{\lambda k_i}$, $\tilde{C}_{\lambda k_i}$, $\tilde{N_{\lambda k_i}}$ and $\tilde{H}_{\lambda k_i}$ are dynamic terms scaled by k_i at timestamp t_j, "sat" is the saturation for exoskeleton torque, E_{ref} and E_{closed} are energy-related terms of the reference model (7) and closed-loop system (4) at timestamp t_j, respectively. In this paper, we defined E_{ref} and E_{closed} to be kinetic energies, total energies, and Lagrangians for both (7) and (4). Because we scaled inertial parameters in M to define $\tilde{M}_{\lambda k_i}$, it still represents the inertia matrix of a robot with different masses and inertia, thus the positive definite property always holds true [25]. The MATLAB function **fmincon** was used to acquire the parameter k_i.

Between two adjacent timestamps, we used a GPR model to interpolate values for k_i [26] and calculate control law (6). We assume $k_i(q(t_j), \dot{q}(t_j))$ is distributed as a Gaussian process, i.e.,

$$k_i(q(t_j), \dot{q}(t_j)) = \text{Gaussian Process}(\mu, \sigma), \tag{10}$$

where μ is the expected value for k_i and σ is the covariance matrix that are updated based on values for k_i from the previous step.

C. Outer Layer Optimization

The outer layer is designed to update reference energy's parameters using HIL BO to minimize metabolic cost, i.e.,

$$\begin{aligned} \min_{\alpha_i \in [\alpha_{\min},\ \alpha_{\max}]} \quad & f = E_{\text{meta}} + f_1, \\ \text{s.t.} \quad & \tilde{M}_\lambda\ddot{q} + \tilde{C}_\lambda\dot{q} + \tilde{N}_\lambda = \tilde{H}_\lambda v, \\ & \text{eig}(\tilde{M}_\lambda) > 0, \end{aligned}$$

where $\alpha_i > 0$ is bounded within $[\alpha_{\min}, \alpha_{\max}]$ to exclude excessive exoskeleton torques. The cost function f consists of two parts: a metabolic cost function E_{meta} and a penalty function f_1. In this paper, we adopted a simulation-based metric by assuming human joint torque square is proportional to the muscle activation [27]:

$$E_{\text{meta}} = \frac{\int_0^T v_i^2(t)\text{d}t}{T(mgl)^2} \approx \frac{\sum_{j=1}^{N_T} v_i^2(j)\Delta t}{T(mgl)^2}, \tag{11}$$

where T is the step time period, v_i is the human joint torque, N_T is the number of timesteps in the simulation, m is the overall mass of the biped, l is the length of the biped leg, and g is the gravitational constant.

We included f_1 in the cost function to penalize unstable cases during walking. In this paper, we check the stability numerically through examining the eigenvalues of the linearized Poincaré map $\mathcal{P} : \mathcal{S} \to \mathcal{S}$, where $x^* = \mathcal{P}(x^*)$ is the intersection point between periodic orbits and the switching surface $\mathcal{S}$ from one step to the successive step. If eigenvalues of the linearized Poincare map $\nabla_x\mathcal{P}(x^*)$ at the fixed point x^* are within the unit circle, the periodic orbit $\mathcal{O}$ is exponentially stable [28]. The function f_1 is therefore defined as

$$f_1 = \begin{cases} 0 & |\text{eig}(\nabla_x\mathcal{P}(x^*))|_{\max} < 1, \\ \beta\ln(|\text{eig}(\nabla_x\mathcal{P}(x^*))|_{\max}) & |\text{eig}(\nabla_x\mathcal{P}(x^*))|_{\max} \geq 1, \end{cases}$$

where $\beta > 0$ is the punishment coefficient. Pseudocode for the overall optimization framework can be found in Algorithms 1

Authorized licensed use limited to: CLEMSON UNIVERSITY. Downloaded on February 19,2024 at 20:01:40 UTC from IEEE Xplore. Restrictions apply.

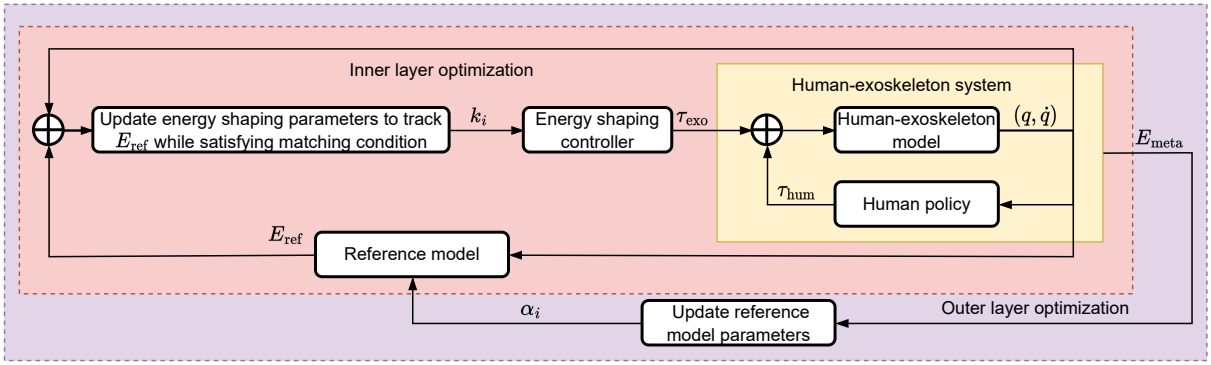

Fig. 1. Overall diagram of the two-layer optimization framework. Highlighted regions in yellow, pink, and purple indicate the human-exoskeleton system, inner loop, and outer loop of the framework, respectively. We used the MATLAB function **fmincon** in the inner loop to find the energy shaping parameters k_i that satisfy the matching condition, and HIL BO in the outer loop to update the reference energy's parameters α_i.

and 2. In Algorithm 2, $P(f)$ is the Gaussian process prior distribution model, $P(f|D)$ is the posterior distribution defined based on the set D which includes reference model parameters and values of f, and $A(\alpha|P(f|D))$ is the acquisition function that selects the next reference model parameters [29].

Algorithm 1 Inner Layer Optimization

Initialize state $(q(t_0),\ \dot{q}(t_0))$;
for Timestamp t_j, $j = 0, 1, \cdots,\ T$ **do**
  Calculate reference model energy E_{ref};
  if At selected timestamp **then**
    Use **fmincon** to find parameters k_i;
  else
    Use GPR to interpolate parameters k_i;
  end if
  Calculate energy shaping torque $u(t_j, k_i)$;
  Solve dynamics (4) and update $(q(t_{j+1}),\ \dot{q}(t_{j+1}))$;
end for

IV. Simulation & Discussion

In order to verify the performance of the proposed optimization framework, we conducted simulations on a 4-DoF point-feet and an 8-DoF biped model, both with a torso (Fig. 2), with different combinations of k_i and α_i. Because pelvic anterior and posterior only tilt slightly during human walking [30], we added an angular constraint to the torso so that it is always perpendicular to the walking direction to avoid the definition of extra DoFs. Bipedal locomotion in general can be modeled as a hybrid system with both continuous dynamics and discrete dynamics at impacts [28]. The hybrid dynamics of a general biped can be expressed as

$$\begin{cases} M\ddot{q} + C\dot{q} + N + A^T\lambda = \tau, & q^- \notin \mathcal{S}, \\ \dot{q}^+ = \Delta(\dot{q}^-), & q^- \in \mathcal{S}, \end{cases} \tag{12}$$

where Δ is the associated impact map [28].

A. 4-DoF Biped Model

The generalized coordinates for the 4-DoF biped model are given as $q_{4\text{D}} = (\phi, \theta_k, \theta_h, \theta_{sk})^T \in \mathbb{R}^4$, where ϕ is the angle between the stance shank and the vertical axis, θ_k and θ_{sk} are the stance and swing knee angles, and θ_h is the hip angle. We implicitly modeled the contact constraints in the dynamics so that the term $A^T\lambda$ does not show up in

Algorithm 2 Outer Layer Optimization

Reference energy parameters Initialization: Initialize reference model parameters $\alpha_i(0) \in [\alpha_{\min}, \alpha_{\max}]$;
Optimization initialization: Initialize Bayesian $P(f)$;
Obtain metabolic cost of passive walking $E_{\text{meta}}(0)$;
Calculate the cost value $f(0) = E_{\text{meta}}(0) + f_1(0)$;
for $l = 0, 1, \cdots,$ iteration **do**
  Update dataset $D = \{(\alpha_i(r), f(r)), r = 0, 1, \cdots, l\}$;
  Perform BO to update $P(f|D)$;
  Select $\alpha_i(l+1) = \arg\max_{\alpha_i}\ A(\alpha_i|D)$;
  Controlled walking to get $E_{\text{meta}}(l+1)$;
  if Unstable **then**
    $f_1(l+1) = \beta \ln(|\text{eig}(\nabla_x \mathcal{P}(x^*))|_{\max})$;
  else if Stable **then**
    $f_1(l+1) = 0$;
  end if
  Calculate the cost value $f(l+1) = E_{\text{meta}}(l+1) + f_1(l+1)$;
end for

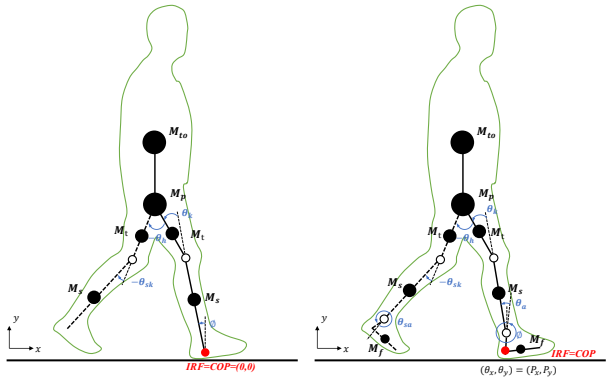

Fig. 2. 4-DoF (left) and 8-DoF (right) biped models used in simulation. The solid lines and dashed lines indicate the stance and swing legs, respectively. The IRFs for both models are defined at the biped's stance foot.

Authorized licensed use limited to: CLEMSON UNIVERSITY. Downloaded on February 19,2024 at 20:01:40 UTC from IEEE Xplore. Restrictions apply.

the EoM. We assumed both knee and stance ankle joints are actuated by human as well as exoskeleton torques, i.e., $\tau_{\mathrm{hum-4D}} = [0, v_k, v_h, v_{sk}]^T \in \mathbb{R}^4$, and $\tau_{\mathrm{exo-4D}} = [0, u_k, u_h, u_{sk}]^T \in \mathbb{R}^4$. To approximate human joint torques, we used a Proportional–Derivative (PD) controller $v_i = -K_{\mathrm{Pi}}(q_i - \bar{q}_i) - K_{\mathrm{Di}}\dot{q}_i$, $i \in \{k, h, sk\}$, where K_{Pi} and K_{Di} are the proportional and derivative gain matrices, and $\bar{q}_i$ is the equilibrium point of the i-th joint. During simulation, we first tuned the PD gain matrices to generate a stable limit cycle for the biped walking down slope and then implemented the optimization framework to conduct simulations. For the 4-DoF biped model, We adopted the following ways to define the closed-loop dynamics (4):

Case 1: $(\tilde{m}_{\mathrm{i}}, \tilde{I}_{\mathrm{i}}) = k_1 \cdot (m_{\mathrm{i}}, I_{\mathrm{i}}), i \in \{\text{shank, thigh, hip, torso}\}$

Case 2: $(\tilde{m}_{\mathrm{shank}}, \tilde{I}_{\mathrm{shank}}) = k_1 \cdot (m_{\mathrm{shank}}, I_{\mathrm{shank}})$,
$(\tilde{m}_{\mathrm{i}},\ \tilde{I}_{\mathrm{i}}) = k_2 \cdot (m_{\mathrm{i}}, I_{\mathrm{i}}),\ i \in \{\text{thigh, hip, torso}\}$

Case 3: $(\tilde{m}_{\mathrm{shank}}, \tilde{I}_{\mathrm{shank}}) = k_1 \cdot (m_{\mathrm{shank}}, I_{\mathrm{shank}})$,
$(\tilde{m}_{\mathrm{thigh}}, \tilde{I}_{\mathrm{thigh}}) = k_2 \cdot (m_{\mathrm{thigh}}, I_{\mathrm{thigh}})$,
$(\tilde{m}_{\mathrm{i}}, \tilde{I}_{\mathrm{i}}) = k_3 \cdot (m_{\mathrm{i}}, I_{\mathrm{i}}),\ i \in \{\text{hip, torso}\}$

For defining reference energy E_{ref}, Browning et al. [31] show that adding extra masses at the distal end of human lower extremities will have greater influence on the overall metabolic cost. We therefore embraced this philosophy to separately scale the shank and other limb masses as

$$m^{\mathrm{ref}}_{\mathrm{shank}} = \alpha_1 \cdot m_{\mathrm{shank}},\ I^{\mathrm{ref}}_{\mathrm{shank}} = \alpha_1 \cdot I_{\mathrm{shank}},$$
$$m^{\mathrm{ref}}_i = \alpha_2 \cdot m_{\mathrm{i}},\ I^{\mathrm{ref}}_{\mathrm{i}} = \alpha_2 \cdot I_{\mathrm{i}},\ i \in \{\text{thigh, hip, torso}\}$$

B. 8-DoF Biped Model

The generalized coordinates of the 8-DoF biped model are given as $q_{8\mathrm{D}} = (p_x, p_y, \phi, \theta_a, \theta_k, \theta_h, \theta_{sk}, \theta_{sa})^T \in \mathbb{R}^8$. In addition to the configuration vector for the 4-DoF model, θ_a and θ_{sa} indicate the stance and swing ankle angles, p_x and p_y are the heel coordinates with respect to the IRF. Impacts happen when the swing heel contacts the ground and subsequently when the stance foot slaps the ground. The human input torque vector is $\tau_{\mathrm{hum-8D}} = [0_{1\times3}, v_a, v_k, v_h, v_{sk}, v_{sa}]^T \in \mathbb{R}^8$, where each joint torque $v_i,\ i \in \{a, k, h, sk, sa\}$ is defined as a PD controller as in Sec. IV-A. All these joints are also actuated by the exoskeleton torque, i.e., $\tau_{\mathrm{exo-8D}} = [0_{1\times3}, u_a, u_k, u_h, u_{sk}, u_{sa}]^T \in \mathbb{R}^8$. We defined the desired inertial parameters for (4) to be $(\tilde{m}_i,\ \tilde{I}_i) = k_1 \cdot (m_i, I_i),\ i \in \{\text{foot, shank, thigh, hip, torso}\}$. We chose to define the reference energy for (7) as

$$m^{\mathrm{ref}}_{\mathrm{i}} = \alpha_1 \cdot m_{\mathrm{i}},\ I^{\mathrm{ref}}_{\mathrm{i}} = \alpha_1 \cdot I_{\mathrm{i}},\ i \in \{\text{foot, shank, thigh}\}$$
$$m^{\mathrm{ref}}_{\mathrm{j}} = \alpha_2 \cdot m_{\mathrm{j}},\ I^{\mathrm{ref}}_{\mathrm{j}} = \alpha_2 \cdot I_{\mathrm{j}},\ \mathrm{j} \in \{\text{hip, torso}\}$$

All parameters used for simulation are summarized in Table. I, where "(8)" and "(4)" in the first column indicate the parameters for the 8-DoF and 4-DoF models, respectively.

C. Results & Discussion

Fig. 3 demonstrates values for k_i and energy tracking performance of the 4-DoF biped throughout the optimization process. We scaled the inertial parameters to define (4) following Cases 1 to 3 in Sec. IV-A, and E_{closed} and E_{ref} were chosen as the total energy for (4) and (7) in f_{inner}, respectively. From this figure, we can see that when less than two energy shaping parameters were used (i.e., k_1 and k_2), the proposed algorithm quickly (within four steps) finds their values that satisfied the matching condition (5) in the inner layer. When three energy shaping parameters were selected, the increase in parameter numbers provides more options for satisfying the matching condition, therefore trajectories of k_i do not exhibit periodic behaviors. For all cases, the closed-loop energy well tracks the reference energy, except for the slight fluctuation in the third case.

Fig. 4 depicts the relationship between cost function value f and the reference parameters α_1 and α_2 for the 8-DoF biped, where E_{closed} and E_{ref} were chosen as the Lagrangian of (4) and (7) in f_{inner}. The results indicate that the cost function value decreases with the reduction of α_1 and α_2. This coincides with the experimental results in [24] that reducing masses on human limbs decreases metabolic costs during walking. In addition, body segments associated with α_2 (hip and torso) play a more dominant role in determining the values for the cost function f. The optimal cost function value is indicated by the red "*" that lies between $\alpha_1 \in [0.8, 1]$

TABLE I
BIPED MODEL AND SIMULATION PARAMETERS

Parameter	Variable	Value
Torso mass	m_{to}	25.07 [kg]
Hip mass	m_{h}	6.66 [kg]
Thigh mass	m_{t}	9.457 [kg]
Thigh moment of inertia	I_{t}	0.1995 [kg·m^2]
Shank moment of inertia	I_{s}	0.0369 [kg·m^2]
Shank mass (4)	m_{s}	5.053 [kg]
Shank mass (8)	m_{s}	4.053 [kg]
Foot mass (8)	m_{f}	1 [kg]
Slope angle	γ	0.095 [rad]
Full biped torso length	l_{to}	0.504 [m]
Full biped thigh length	l_{t}	0.428 [m]
Full biped shank length (4)	l_{s}	0.435 [m]
Full biped shank length (8)	l_{s}	0.428 [m]
Full biped heel length (8)	l_{a}	0.07 [m]
Full biped foot length (8)	l_{f}	0.2 [m]
Hip equilibrium	$\bar{q}_{\mathrm{h}}$	−0.5 [rad]
Stance knee equilibrium	$\bar{q}_{\mathrm{k}}$	−0.05 [rad]
Swing knee equilibrium (4)	$\bar{q}_{\mathrm{sk}}$	0.01 [rad]
Hip proportional gain (4)	K_{ph}	101.05 [N·m/rad]
Hip derivative gain (4)	K_{dh}	13.07 [N·m·s/rad]
Swing knee proportional gain (4)	K_{psk}	121.26 [N·m/rad]
Swing knee derivative gain (4)	K_{dsk}	14.07 [N·m·s/rad]
Stance knee proportional gain (4)	K_{pk}	303.15 [N·m/rad]
Stance knee derivative gain (4)	K_{dk}	15.84 [N·m·s/rad]
Swing knee equilibrium (8)	$\bar{q}_{\mathrm{sk}}$	0.2 [rad]
Swing ankle equilibrium (8)	$\bar{q}_{\mathrm{sa}}$	−0.25 [rad]
Stance ankle equilibrium (8)	$\bar{q}_{\mathrm{a}}$	0.01 [rad]
Hip proportional gain (8)	K_{ph}	182.250 [N·m/rad]
Hip derivative gain (8)	K_{dh}	35.1 [N·m·s/rad]
Swing knee proportional gain (8)	K_{psk}	182.25 [N·m/rad]
Swing knee derivative gain (8)	K_{dsk}	18.9 [N·m·s/rad]
Swing ankle proportional gain (8)	K_{psa}	145.80 [N·m/rad]
Swing ankle derivative gain (8)	K_{dsa}	0.81 [N·m·s/rad]
Stance ankle proportional gain (8)	K_{pa}	486.00 [N·m/rad]
Stance ankle derivative gain (8)	K_{da}	18.52 [N·m·s/rad]
Stance knee proportional gain (8)	K_{pk}	486.00 [N·m/rad]
Stance knee derivative gain (8)	K_{dk}	18.52 [N·m·s/rad]

Authorized licensed use limited to: CLEMSON UNIVERSITY. Downloaded on February 19,2024 at 20:01:40 UTC from IEEE Xplore. Restrictions apply.

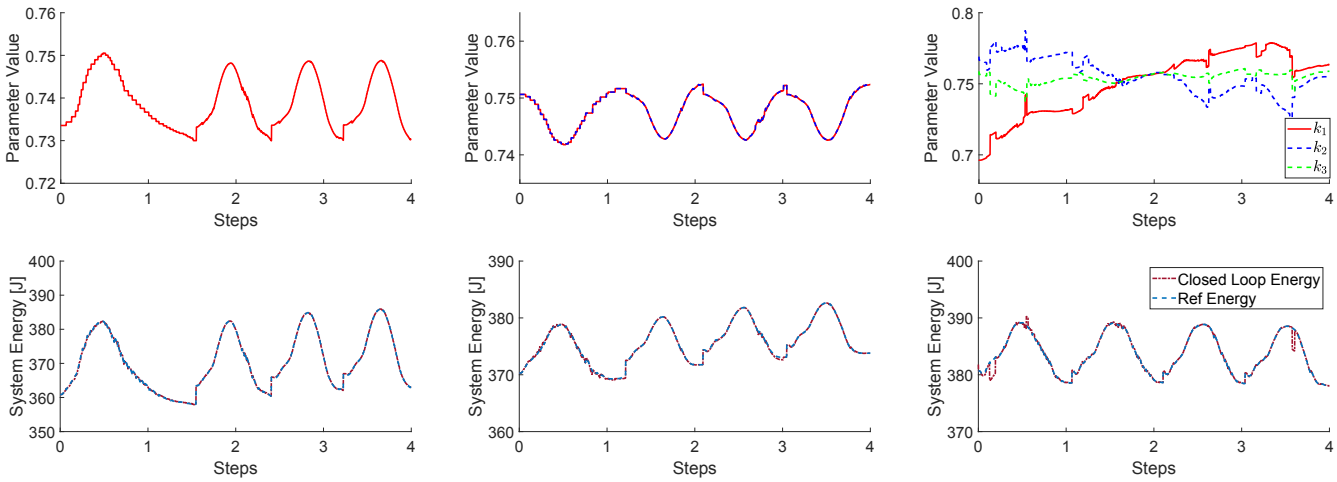

Fig. 3. Evolution of k_i throughout the customization process (top row) and the associated total energy tracking (bottom row) for the 4-DoF model (Left to right: Case 1, 2, and 3 as defined in Sec. IV-A).

and $\alpha_2 = 0.6$. Due to the passive nature of the simulation biped, we can only reduce inertial parameters of (7) to a certain degree, after which there will be insufficient energy to maintain a stable gait. The singular point in the top-right corner and the bottom-left region (black dots) indicates unstable cases, where the penalty function penalizes the unstable cases to increase the value f.

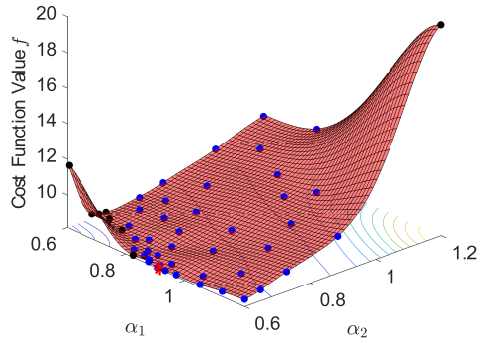

Fig. 4. Relationship between cost function f and reference model parameters α_1 and α_2 for the 8-DoF biped. The optimal value of the cost function f is indicated by the red " $*$ " after 50 times BO iteration.

Fig. 5 compares the optimal cost value f with function evaluations for the 8-DoF biped model. We selected E_{ref} and E_{closed} to be the kinetic energy, total energy, and Lagrangian for dynamics (7) and (4) in f_{inner}, respectively. For each case, BO evaluated the cost function 20 times before getting a steady value of the cost function, where we let the biped walk for 10 steps before calculating the human metabolic cost. The results show that f of all cases converged to a steady value within 200 steps.

Metabolic cost reductions of both the 4-DoF and 8-DoF bipeds with different energy tracking cases are shown in Fig. 6. Because human anatomical parameters are difficult to be measured accurately, we therefore added random numbers with mean value 1 and standard deviation 0.02 as noises to each of the human inertial parameters to incorporate parametric errors. Adding such noises is equivalent to adding $\pm 5\%$ uncertainty to each of the inertial parameters, which

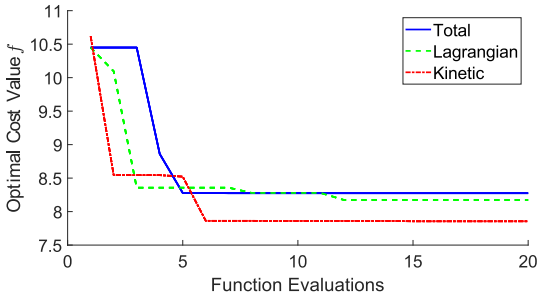

Fig. 5. Optimal cost value f vs. function evaluations for kinetic energy, total energy and Lagrangian tracking of the 8-DoF biped.

is considered to be acceptable in past biomechanics studies [32], [33]. From Fig. 6, we can see that tracking the kinetic energy, total energy, and Lagrangian of the reference model (7) all rendered metabolic cost reduction, among which kinetic energy tracking rendered the most metabolic reduction. For comparison, we also simulated the metabolic cost on an 8-DoF model that has the same configuration as the one in Fig. 2 but without the torso. Having a torso will help the biped better maintain balance, and the torso mass is dominant compared to other leg segments, thus shaping the torso mass is beneficial in assisting human gaits. The associated optimal reference energy parameters are shown in Fig. 7.

Finally, we plotted the exoskeleton torques using an able-bodied subject's kinematic data from [34] and the optimized parameter k_1 for all inertial parameters based on the 8-DoF model in Fig. 8. We defined E_{closed} and E_{ref} in f_{inner} to be the kinetic energy (blue), total energy (green), and Lagrangian (black) of (4) and (7), respectively. We can see that for all cases, the calculated exoskeleton torques highly approximate real human biological torques, which is beneficial as the optimized parameters will enable exoskeletons to compensate for human joint torques that could possibly lead to human effort reduction in practice.

V. CONCLUSIONS & FUTURE WORK

This paper proposed a two-layer, HIL optimization framework for customizing exoskeleton assistance. The inner-layer

Authorized licensed use limited to: CLEMSON UNIVERSITY. Downloaded on February 19,2024 at 20:01:40 UTC from IEEE Xplore. Restrictions apply.

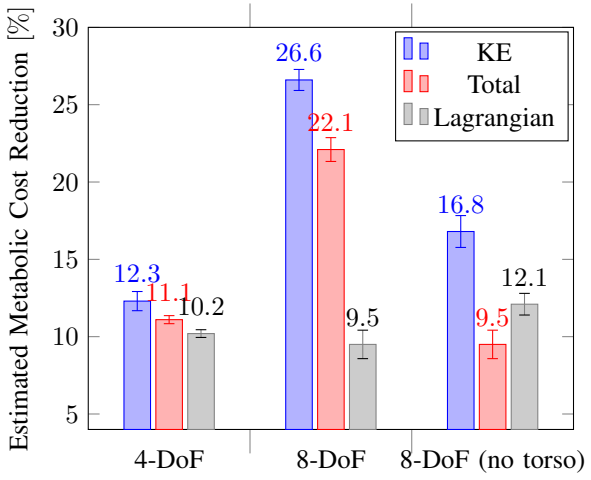

Fig. 6. Metabolic cost reduction (mean $\pm 1\cdot$ standard deviation) compared to passive gaits of the 4-DoF (left), 8-DoF (center), and 8-DoF without torso biped (right) models. We used one single value k_i to scale all the inertial parameters for each biped model.

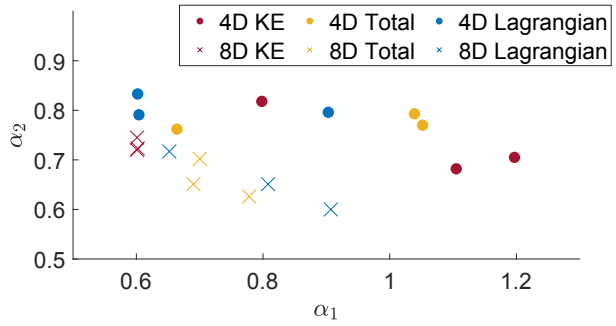

Fig. 7. Optimal reference energy parameters α_1 and α_2 for the 4-DoF and 8-DoF biped models.

is designed to find solutions of the matching condition and tracks a virtual reference model's energy, which is defined based on a human subject's self-selected gaits and scaled anatomical parameters. The outer layer adopts HIL-based BO to update the reference energy for minimizing metabolic costs. Simulation results on two biped models demonstrated the efficacy of the proposed framework, i.e., it was able to find solutions to the matching condition and tracks the defined reference energy, meanwhile the generated exoskeleton assistance reduced metabolic costs. Moreover, exoskeleton torques calculated using an able-bodied joint kinematics with customized energy shaping parameters highly align with human biological torques. Future work includes refining the framework to find solutions to the matching condition along the entire trajectory of the model states, conducting passivity and stability analyses, and experimentation on physical applications.

References

[1] R. Baud, A. R. Manzoori, A. Ijspeert, and M. Bouri, "Review of control strategies for lower-limb exoskeletons to assist gait," *J. NeuroEng. Rehabil.*, vol. 18, no. 1, pp. 1–34, 2021.

[2] D. Pinto-Fernandez, D. Torricelli, M. del Carmen Sanchez-Villamanan, F. Aller, K. Mombaur, R. Conti, N. Vitiello, J. C. Moreno, and J. L. Pons, "Performance evaluation of lower limb exoskeletons: a systematic review," *IEEE Trans. Neural Syst. Rehabil. Eng.*, vol. 28, no. 7, pp. 1573–1583, 2020.

[3] A. Rodríguez-Fernández, J. Lobo-Prat, and J. M. Font-Llagunes, "Systematic review on wearable lower-limb exoskeletons for gait training in neuromuscular impairments," *J. NeuroEng. Rehabil.*, vol. 18, no. 1, pp. 1–21, 2021.

[4] V. Bartenbach, M. Gort, and R. Riener, "Concept and design of a modular lower limb exoskeleton," in *6th IEEE Int. Conf. on BioRob*, 2016, pp. 649–654.

[5] H. Hsu, I. Kang, and A. J. Young, "Design and evaluation of a proportional myoelectric controller for hip exoskeletons during walking," in *Dynamic Systems and Control Conference*, vol. 51890. American Society of Mechanical Engineers, 2018, p. V001T13A005.

[6] S. Y. Gordleeva, S. A. Lobov, N. A. Grigorev, A. O. Savosenkov, M. O. Shamshin, M. V. Lukoyanov, M. A. Khoruzhko, and V. B. Kazantsev, "Real-time EEG–EMG human–machine interface-based control system for a lower-limb exoskeleton," *IEEE Access*, vol. 8, pp. 84 070–84 081, 2020.

[7] A. J. Young and D. P. Ferris, "State of the art and future directions for lower limb robotic exoskeletons," *IEEE Trans. Neural Syst. Rehabil. Eng.*, vol. 25, no. 2, pp. 171–182, 2016.

[8] M. K. Shepherd and E. J. Rouse, "Design and validation of a torque-controllable knee exoskeleton for sit-to-stand assistance," *IEEE/ASME Trans. Mechatron.*, vol. 22, no. 4, pp. 1695–1704, 2017.

[9] W. Ma, H. Cheng, R. Huang, and Q. Chen, "Gait planning with dynamic movement primitives for lower limb exoskeleton walking upstairs," in *IEEE Int. Conf. Robot. Biomim*, Dec. 2018, pp. 703–708.

[10] G. Lv, J. Lin, and R. D. Gregg, "Trajectory-free control of lower-limb exoskeletons through underactuated total energy shaping," *IEEE Access*, vol. 9, pp. 95 427–95 443, 2021.

[11] J. Lin, G. Lv, and R. D. Gregg, "Contact-invariant total energy shaping control for powered exoskeletons," in *American Control Conference*, 2019, pp. 664–670.

[12] G. Viola, R. Ortega, R. Banavar, J. Á. Acosta, and A. Astolfi, "Total energy shaping control of mechanical systems: simplifying the matching equations via coordinate changes," *IEEE Trans. Autom. Control*, vol. 52, no. 6, pp. 1093–1099, 2007.

[13] A. M. Bloch, N. E. Leonard, and J. E. Marsden, "Controlled Lagrangians and the stabilization of mechanical systems. I. the first matching theorem," *IEEE Trans. Autom. Control*, vol. 45, no. 12, pp. 2253–2270, 2000.

[14] P. S. Gandhi, P. Borja, and R. Ortega, "Energy shaping control of an inverted flexible pendulum fixed to a cart," *Control Engineering Practice*, vol. 56, pp. 27–36, 2016.

[15] F. Andreev, D. Auckly, S. Gosavi, L. Kapitanski, A. Kelkar, and W. White, "Matching, linear systems, and the ball and beam," *Automatica*, vol. 38, no. 12, pp. 2147–2152, 2002.

[16] G. Lv, H. Zhu, and R. D. Gregg, "On the design and control of highly backdrivable lower-limb exoskeletons: A discussion of past and ongoing work," *IEEE Control Syst. Mag.*, vol. 38, no. 6, pp. 88–113, 2018.

[17] W. Liu, R. Wu, J. Si, and H. Huang, "A new robotic knee impedance control parameter optimization method facilitated by inverse reinforcement learning," *IEEE Rob. Autom. Lett.*, 2022.

[18] Y. Ding, M. Kim, S. Kuindersma, and C. J. Walsh, "Human-in-the-loop optimization of hip assistance with a soft exosuit during walking," *Science robotics*, vol. 3, no. 15, p. eaar5438, 2018.

[19] J. Zhang, P. Fiers, K. A. Witte, R. W. Jackson, K. L. Poggensee, C. G. Atkeson, and S. H. Collins, "Human-in-the-loop optimization of exoskeleton assistance during walking," *Science*, vol. 356, no. 6344, pp. 1280–1284, 2017.

[20] D. F. Gordon, C. McGreavy, A. Christou, and S. Vijayakumar, "Human-in-the-loop optimization of exoskeleton assistance via online simulation of metabolic cost," *IEEE Trans. Rob.*, vol. 38, no. 3, pp. 1410–1429, 2022.

[21] Q. Zhang, V. Nalam, X. Tu, M. Li, J. Si, M. D. Lewek, and H. H. Huang, "Imposing healthy hip motion pattern and range by exoskeleton control for individualized assistance," *IEEE Robot. Autom. Lett.*, vol. 7, no. 4, pp. 11 126–11 133, 2022.

[22] T. Chyou, G. Liddell, and M. Paulin, "An upper-body can improve the stability and efficiency of passive dynamic walking," *J. Theor. Biol.*, vol. 285, no. 1, pp. 126–135, 2011.

[23] G. Lv and R. D. Gregg, "Underactuated potential energy shaping with contact constraints: Application to a powered knee-ankle orthosis," *IEEE Trans. Control Syst. Technol.*, vol. 26, no. 1, pp. 181–193, 2017.

Authorized licensed use limited to: CLEMSON UNIVERSITY. Downloaded on February 19,2024 at 20:01:40 UTC from IEEE Xplore. Restrictions apply.

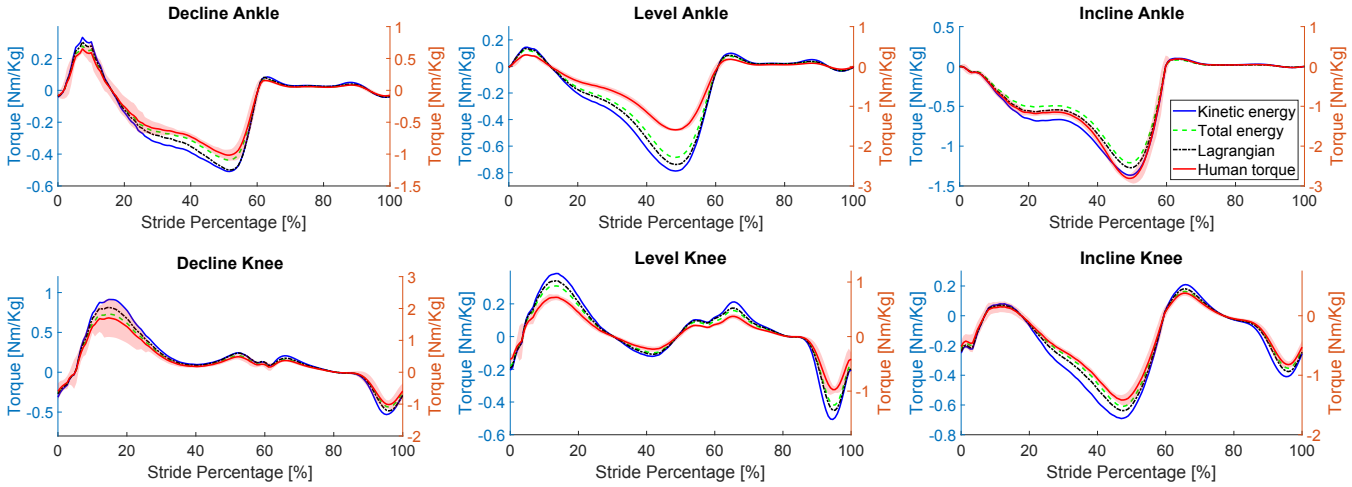

Fig. 8. Human biological torques (red, mean ± 1 standard deviation, [34]) and exoskeleton torques calculated using an able-bodied subject's joint kinematics from [34]. From left to right, the subject walked on the 10° decline, level ground and 10° incline with velocity $1.2\ \mathrm{m/s}$. A single energy shaping parameter k_1 was used to scale all inertial parameters for the 8-DoF biped.

[24] S. Faraji, A. R. Wu, and A. J. Ijspeert, "A simple model of mechanical effects to estimate metabolic cost of human walking," *Sci. Rep.*, vol. 8, no. 1, pp. 1–12, 2018.

[25] R. D. Gregg and M. W. Spong, "Reduction-based control of three-dimensional bipedal walking robots," *Int. J. Robot. Res.*, vol. 29, no. 6, pp. 680–702, 2010.

[26] M. Mukadam, X. Yan, and B. Boots, "Gaussian process motion planning," in *IEEE Int. Conf. Robot. Autom.*, 2016, pp. 9–15.

[27] A. E. Martin and J. P. Schmiedeler, "Predicting human walking gaits with a simple planar model," *J. Biomech.*, vol. 47, no. 6, pp. 1416–1421, 2014.

[28] E. R. Westervelt, J. W. Grizzle, C. Chevallereau, J. H. Choi, and B. Morris, *Feedback Control of Dynamic Bipedal Robot Locomotion*. CRC press, 2018.

[29] M. Kim, Y. Ding, P. Malcolm, J. Speeckaert, C. J. Siviy, C. J. Walsh, and S. Kuindersma, "Human-in-the-loop bayesian optimization of wearable device parameters," *PloS One*, vol. 12, no. 9, p. e0184054, 2017.

[30] M. Jacquelin Perry, "Gait analysis: normal and pathological function," *New Jersey: SLACK*, 2010.

[31] R. C. Browning, J. R. Modica, R. Kram, A. Goswami *et al.*, "The effects of adding mass to the legs on the energetics and biomechanics of walking," *Medicine and science in sports and exercise*, vol. 39, no. 3, p. 515, 2007.

[32] M. T. Pain and J. H. Challis, "High resolution determination of body segment inertial parameters and their variation due to soft tissue motion," *J Appl Biomech*, vol. 17, no. 4, pp. 326–334, 2001.

[33] C. Caulcrick, W. Huo, W. Hoult, and R. Vaidyanathan, "Human joint torque modelling with mmg and emg during lower limb human-exoskeleton interaction," *IEEE Rob. Autom. Lett.*, vol. 6, no. 4, pp. 7185–7192, 2021.

[34] K. R. Embry, D. J. Villarreal, R. L. Macaluso, and R. D. Gregg, "Modeling the kinematics of human locomotion over continuously varying speeds and inclines," *IEEE Trans. Neural Syst. Rehabil. Eng.*, vol. 26, no. 12, pp. 2342–2350, 2018.

Authorized licensed use limited to: CLEMSON UNIVERSITY. Downloaded on February 19,2024 at 20:01:40 UTC from IEEE Xplore. Restrictions apply.